

Quantum lattice-gas model for the Burgers equation

Jeffrey Yepez*

Air Force Research Laboratory
29 Randolph Road, Hanscom AFB, Massachusetts 01731
Jeffrey.Yepez@hanscom.af.mil
<http://qubit.plh.af.mil/>

June 28, 2000

Abstract

A quantum algorithm is presented for modeling the time evolution of a continuous field governed by the nonlinear Burgers equation in one spatial dimension. It is a microscopic-scale algorithm for a type-II quantum computer, a large lattice of small quantum computers interconnected in nearest neighbor fashion by classical communication channels. A formula for quantum state preparation is presented. The unitary evolution is governed by a conservative quantum gate applied to each node of the lattice independently. Following each quantum gate operation, ensemble measurements over independent microscopic realizations are made resulting in a finite-difference Boltzmann equation at the mesoscopic scale. The measured values are then used to re-prepare the quantum state and one time step is completed. The procedure of state preparation, quantum gate application, and ensemble measurement is continued ad infinitum. The Burgers equation is derived as an effective field theory governing the behavior of the quantum computer at its macroscopic scale where both the lattice cell size and the time step interval become infinitesimal. A numerical simulation of shock formation is carried out and agrees with the exact analytical solution.

Keywords: quantum lattice gas; type-II quantum computer; Burgers equation

*This research reported in this paper was carried out under the quantum computing initiative underway at the Air Force Research Laboratory and supported by the Air Force Office of Scientific Research. This paper was presented at the 9th International Conference on Discrete Simulation of Fluid Dynamics on August 21, 2000.

1 Introduction

This paper presents a quantum algorithm for modeling the nonlinear Burgers equation. This represents a strong numerical test of the modeling utility of quantum computers because the Burgers equation is a difficult nonlinear partial differential equation to accurately model without numerical instabilities. Its applications to turbulence, intermittency, structures in a self-gravitating medium [1] and shock formation in inelastic gases [2] gives the Burgers equation unique importance in the field of computational physics. One of the goals of this paper is to place the question of modeling the Burgers equation into the emerging field of quantum computational physics.

The quantum algorithm presented here is suited to a type-II quantum computing architecture that is a large array of small quantum computers interconnected by classical communication channels [3]. The quantum algorithm is based on the *factorized quantum lattice-gas method*, which has been previously applied to modeling the Navier-Stokes equations of fluid dynamics [4, 5] and the diffusion equation [6].

Other types of quantum lattice gases appear in the literature, beginning in the mid 1990's, by Succi [7, 8], Bialynicki-Birula [9], Meyer [10, 11], and Boghosian and Taylor [12] to model the relativistic Dirac equation and the nonrelativistic Schrodinger equation, and Yepey [13] to model phase-coherent quantum systems. In contrast, the mesoscopic scale behavior of the factorized quantum lattice gas presented here is purely classical in nature, even though the microscopic scale dynamics is quantum mechanical. This is because measurements are made on each qubit of the quantum computer after each and every application of a local quantum mechanical program independently applied on each site or node of the system. The usefulness of this approach is that practical and efficient computation can be carried out at the mesoscopic scale by an emergent finite-difference Boltzmann transport equation to model a broad class of effective field theories in an unconditionally stable manner. The measurement process in effect “factorizes” the collision term in the lattice-Boltzmann equation so that quantum superpositions and entanglement cannot spread throughout the quantum computer. This keeps quantum superposition and entanglement localized within the lattice nodes for a short duration of time less than the spin-spin decoherence time of the physical system in question.¹ In this way, the measurement process mitigates against any uncontrolled decoherence mechanisms that would otherwise destroy the phase coherence of the quantum computer's wavefunction.

The dynamical evolution of the type-II quantum computer can be described at three spacetime scales, the microscopic, mesoscopic, and macroscopic scales.

¹ Nuclear spins precess at a frequency of $\omega = \frac{geB}{mc}$ about the externally applied magnetic field B . They can precess in phase with each other only for a characteristic time called the *spin-spin decoherence time* and usually denoted by T_2 . Moreover, the *relaxation time* usually denoted T_1 , which is greater than T_2 , is the characteristic time required for the spins to relax back to the energy eigenstates of the two-level spin-system, where these two eigenstates are populated according to the Boltzmann equilibrium occupancy probabilities.

At the microscopic scale, all the quantum dynamics occurs on a discrete spatial lattice. The Hamiltonian of the quantum system is an artificial one; that is, it is produced by a program of externally applied controls. In effect the naturally occurring quantum system is coaxed to act like another quantum system on a discrete lattice with a Hamiltonian of our choosing. One can then describe the dynamical behavior of the “programmed” quantum system at a mesoscopic scale. To do this, an ensemble measurement over identical microscopic realizations is made to determine the occupancy of the two-level energy eigenstates of each qubit in the system. A scaling estimate for the minimum required ensemble size is given in Appendix A. In this way a discrete field of probabilities is obtained, one probability per qubit. At this mesoscopic scale, the occupancy probabilities are defined only on the lattice points, so these probabilities constitute a discrete field of real-valued quantities. A lattice Boltzmann equation for kinetic transport exactly governs the dynamical evolution of this spatially discrete probability field.

Finally, to bridge the gap to the macroscopic scale, the occupancy probabilities at each site of the lattice are summed together to determine what is called a *number density field*. As the number of lattice points increases towards an infinite spatial resolution, which is called the *continuum limit*, the number density field becomes a continuous and differentiable field. Its dynamical evolution can then be approximately described, to any order of desired precision, by a partial differential equation of motion. Since this equation of motion is chosen by construction, for example say it is the Burgers equation, we consider the type-II quantum computer to be a model of the physical system described by that equation of motion. In this sense, the microscopic quantum mechanical system is programmed to act like one particular classical physical system at its macroscopic scale. Therefore, in essence, we exploit quantum mechanics for the purpose of efficient analog computation.

The quantum algorithm presented here is the simplest example of using a quantum computer to solve a one-dimensional nonlinear partial differential equation. To do this, only two qubits are needed at each node of the type-II quantum computer and a single quantum gate is simultaneously and independently applied to all the nodes. In general, to solve nonlinear partial differential equations in two and three-dimensional, more than two qubits per node is required. The minimum number of qubits required for various nonlinear systems, including the Burgers equation, in two and three-dimensions is presently unknown. Furthermore, to correctly and accurately model complex three-dimensional dynamical systems to handle the nonlinear motions of singular boundaries, such as arise in shock fronts, phase and species interfaces, and the like, than many hundreds or thousands of bits may be required per site.² Since the number of particle

² It is possible to estimate the number of qubits required per node based on the bit density of classical lattice-gas models since they are a special case of quantum lattice-gas models. For the Navier-Stokes equation, 6 and 24 bits are needed in two and three-dimensions, respectively, in single speed models of incompressible subsonic flow [14, 15]. To repair anomalies, such as a lack of Galilean invariance, many additional bits are needed to encode the occupancy of a particle and this causes the bit density to be multiplied [16]. If many-speed models are

configurations grows exponentially in the number of on-site bits, implementing the collision process on a classical computer quickly becomes intractable for complicated models.

A speedup due to quantum parallelism is a salient characteristic of a type-II quantum computer despite the periodic measurement process. This speedup occurs even though the quantum mechanical superposition of states is restricted to only a sub-manifold of the full Hilbert space. With a type-II quantum computer, in principle, it is possible to gain a speedup because the computational work required to implement the collision process is order unity in certain cases. This is possible because the Hamiltonian (say an Ising spin system with nearest neighbor interaction) governing the evolution of a node conserves certain quantities, such as the total magnetization along an external applied uniform magnetic field. In the quantum lattice-gas model presented in this paper, the total magnetization is mapped on to a field quantity that is governed by the Burgers equation in the continuum limit. Therefore, once the appropriate quantum state preparation is completed on each node of the type-II quantum computer, only one unitary transformation step is needed before the quantum state of each qubit is measured. By refocusing two-spin interactions in a nuclear magnetic resonance quantum computer [23], the collision process can therefore be efficiently computed. Other conserved quantities of the on-site Hamiltonian may be mapped to recover the macroscopic-scale evolution of additional field quantities. For example, the square of the total spin may be mapped on a conserved local momentum vector to recover nonlinear hydrodynamic flow.

2 Factorized Quantum Lattice-Gas Algorithm

2.1 Step 1: Computational Memory State Encoding

Consider a one-dimensional lattice with L sites. Each site of the lattice is labeled by a coordinate x_l , where $l = 1, \dots, L$. To model the Burgers equation, we use two qubits physically located at each site of the lattice. Note that in this case of only two qubits per node, an exponential speedup of the algorithm implemented on a type-II quantum computer versus a classical computer would not be realized [6]. To realize the exponential speedup, many more than two qubit per node is required. Therefore, this quantum algorithm is simply a test case, and to exploit quantum efficiency one must consider a generalized two or three-dimensional version of the algorithm presented here.

considered for compressible subsonic flow, the required number bits per node are doubled or tripled [17]. To handle compressible transonic and supersonic flows, many additional bits are necessary to handle the large distance advections of local flows [18]. Furthermore, to handle multiphase fluids, additional bits are required to communicate long-range inter-particle forces [19]. An efficient implementation of a multiphase fluid requires doubling the bit density as a hydrodynamic lattice-gas model is generalized to a multiphase hydrodynamic model. That is, for every bit in the original model encoding a particle's occupancy, an additional messenger bit is added to handle the long-range force that acts on that particle [20]. The bit density also doubles as one adds another species, as is done in models of immiscible fluids and microemulsions [21] or reactive systems [22].

With two qubits per node, there are a total $2L$ qubits in the type-II quantum computer. These qubits are denoted by the ket $|q_a(x_l, t_o)\rangle$, where $a = 1, 2$. The *computational memory state* of the type-II quantum computer is encoded in the quantum wave function, $|\Psi(x_1, x_2, \dots, x_L, t_o)\rangle$, in a particular fashion described here. First of all, it is important to note that the quantum wave function of a type-II quantum computer is always expressible in tensor product form

$$|\Psi(x_1, x_2, \dots, x_L, t_o)\rangle = \bigotimes_{l=1}^L |\psi(x_l, t_o)\rangle. \quad (1)$$

The ket $|\psi(x_l, t_o)\rangle$ is called the *on-site ket*. In general, with b qubits per node, the *computational manifold* is $L2^b$ -dimensional, which is a small fraction of the full 2^{Lb} -dimensional Hilbert space when the number of lattice sites L is large. In our present case with $b = 2$ qubits per site, the computational manifold is of size $L2^2$. Each on-site ket resides in a 2^2 -dimensional subspace of the computational manifold.

Let us choose the following four basis states in the number representation

$$|00\rangle = \begin{pmatrix} 0 \\ 0 \\ 0 \\ 1 \end{pmatrix} \quad |01\rangle = \begin{pmatrix} 0 \\ 0 \\ 1 \\ 0 \end{pmatrix} \quad |10\rangle = \begin{pmatrix} 0 \\ 1 \\ 0 \\ 0 \end{pmatrix} \quad |11\rangle = \begin{pmatrix} 1 \\ 0 \\ 0 \\ 0 \end{pmatrix}. \quad (2)$$

In this basis, the number operators for the occupancy of qubits $|q_1\rangle$ and $|q_2\rangle$ are respectively represented by the following two matrices

$$\hat{n}_1 = \begin{pmatrix} 1 & 0 & 0 & 0 \\ 0 & 1 & 0 & 0 \\ 0 & 0 & 0 & 0 \\ 0 & 0 & 0 & 0 \end{pmatrix} \quad \hat{n}_2 = \begin{pmatrix} 1 & 0 & 0 & 0 \\ 0 & 0 & 0 & 0 \\ 0 & 0 & 1 & 0 \\ 0 & 0 & 0 & 0 \end{pmatrix}. \quad (3)$$

We are now in a position to say how the computational memory state of the type-II quantum computer is encoded in $|\Psi(x_1, x_2, \dots, x_L, t_o)\rangle$. This is specified by a list of $2L$ probabilities, one probability value for each qubit. Each probability value is supposed to be a continuous real numbered quantity in the range of 0 to 1. In practice however, each probability value can only be approximately represented within the dynamical range physically allowable by the technique used to embody a qubit, for example using the spin state of an atomic nucleus [24, 25] or the state of a fluxon that entered a superconducting quantum interference device through a Josephson junction [26, 27].³ The probability value encoded in each qubit is called the *occupancy probability* and it is denoted by $f_a(x_l, t_o)$ for the a^{th} qubit at site x_l at time t_o .

³ The issue of the achievable dynamical range of physical qubits for encoding probabilities is under study in our laboratory and by our collaborators for the two different cases of type-II quantum computers employing either the nuclear magnetic resonance or superconducting electronics approaches.

Each qubit initially encodes the occupancy probability according to the following prescription

$$|q_a(x_l, t_o)\rangle = \sqrt{f_a(x_l, t_o)}|1\rangle + \sqrt{1 - f_a(x_l, t_o)}|0\rangle, \quad (4)$$

for $l = 1, 2, \dots, L$ and $a = 1, 2$. Equation (4) represents the first step of the quantum lattice-gas algorithm.⁴ This is called *state preparation* and defines the way we write data to the type-II quantum computer's memory. Since initially each on-site ket is a tensor product over the qubits at the site, $|\psi\rangle = |q_1\rangle \otimes |q_2\rangle$, the on-site ket therefore has the following four components in our chosen basis

$$|\psi(x_l, t_o)\rangle = \sqrt{f_1(x_l, t_o)f_2(x_l, t_o)}|11\rangle + \sqrt{f_1(x_l, t_o)(1 - f_2(x_l, t_o))}|10\rangle + \sqrt{(1 - f_1(x_l, t_o))f_2(x_l, t_o)}|01\rangle + \sqrt{(1 - f_1(x_l, t_o))(1 - f_2(x_l, t_o))}|00\rangle. \quad (5)$$

In this construction of the on-site ket, the qubits are considered to be distinguishable.⁵

The “*number density*” field is defined as the sum of the occupancy probabilities

$$\rho(x_l, t_o) \equiv f_1(x_l, t_o) + f_2(x_l, t_o). \quad (6)$$

The number density field is a spatially discrete field in that it has a value only on the discrete sites of a lattice. However, we may consider the number density field to be a continuous and differentiable field in the continuum limit where the number of lattice sites becomes infinite, $L \rightarrow \infty$ for a lattice of fixed size. The best justification for this consideration comes directly from numerical simulations of the number density field. It is possible to numerically measure the convergence property of a predicted numerical behavior of the model by comparing it with the exact analytical solution of the partial differential equation the system is supposed to model [6]. As the grid resolution is doubled again and again, it has been observed that the quantum lattice-gas model converges with better than second order accuracy in space and first order accuracy in time to the exact solution [6]. In fact, in a phase-coherent for model of the many-body Schroedinger wave equation, the quantum lattice-gas method is fourth order accurate in space [28]. This high degree of accuracy is not typical of time-explicit dynamical models where the field values at some time step are computed with only knowledge of the field values at the previous time step. The reason for the high-degree of accuracy arises from the fact that the collision process in a unitary one and the resulting mesoscopic kinetic transport equations obey the principle of detailed-balance.

⁴ Note that in general the quantum state of a qubit is determined by three real parameters, an overall phase factor, plus two “Euler” angles specifying its orientation on the unit Bloch sphere, $|q\rangle = e^{i\varphi}(\cos\theta|1\rangle + e^{i\varepsilon}\sin\theta|0\rangle)$. In our case, the overall phase factor, φ , and the internal phase factor, ε , are not used and we simply set $f_a = \cos^2\theta$.

⁵ In the case where the on-site qubits are indistinguishable and fermionic in character, then one must keep track of the the “internal” location of the individual qubits within each node to ensure that the on-kit is antisymmetric. In our present case with two qubits per node, say the qubits are located at the internal locations y_1 and y_2 . Then, the on-site ket would be intialized as $|\psi\rangle = [|q_1\rangle(y_1) \otimes |q_2(y_2)\rangle - |q_1(y_2)\rangle \otimes |q_2(y_1)\rangle]/\sqrt{2}$. In the general case, with more than two qubits per node, a Slater determinant would be used to determine the signs of all the terms contributing to the antisymmetric on-site ket.

2.2 Step 2: Unitary Quantum Evolution

It is necessary to make a clear distinction between the actual microscopic scale evolution of the type-II quantum computer, which is governed by unitary quantum mechanical evolution, and the effective mesoscopic scale evolution of the type-II quantum computer system, which is non-unitary. The unitary quantum mechanical evolution is determined by a *program* of externally applied controls (for example, a sequence radio-frequency pulses in the case of an NMR-based quantum computer) so that the phase-coherent part of the evolution is governed by a quantum wave equation of a particularly chosen form

$$|\psi'(x_l, t_o)\rangle = \hat{U}|\psi(x_l, t_o)\rangle. \quad (7)$$

The chosen unitary evolution matrix, \hat{U} , is called the *collision operator* and it is applied to each lattice site independently causing local quantum superposition and entanglement of the on-site qubits. In general, \hat{U} is decomposable into a sequence of two-qubit quantum gates [29]. Application of the collision operator, homogeneously and independently across all the lattice sites, is the second step of the quantum lattice-gas algorithm. In practice, the time taken to run the collision operator program must be on the order of the T_2 spin-spin decoherence time of the physical system in questions. In the case of the nuclear magnetic resonance type-II quantum computer, T_2 is on the order of 1 second. The choice of the particular components of \hat{U} determines the form of the partial differential equation the quantum lattice-gas can model as shall be demonstrated in §5. In the context of (7) viewed as a collisional scattering process, the ket $|\psi\rangle$ is called the *incoming ket* and the ket $|\psi'\rangle$ is called the *outgoing ket*.

2.3 Step 3: Measurement

The third step of the quantum lattice-gas algorithm is to measure (that is, to “read”) all the occupancy probabilities. This measurement process is a non-unitary action that destroys all the superpositions and entanglements that may have been caused locally at each site of the lattice by application of \hat{U} . Mathematically, we can express the occupation probabilities in terms of the following matrix element of the number operator

$$f'_a(x_l, t_o) = \langle \psi'(x_l, t_o) | \hat{n}_a | \psi'(x_l, t_o) \rangle, \quad (8)$$

for $a = 1, 2$. The updated values of the occupation probabilities, f'_a , as indicated by the prime superscript, are determined by either repeated measurement or by a single measurement over a statistical ensemble, or both.

2.4 Step 4: Global Data Shifts Using Classical Communication Channels

The fourth step of the quantum lattice-gas algorithm is to shift all the occupancy probability data obtained from the measurement process to their neighboring

sites as follows

$$f_a(x_l, t_1) = f'_a(x_{l+e_a}, t_o), \quad (9)$$

where $e_1 = 1$ and $e_2 = -1$. Notice that after this step, we consider time to be incremented by one unit $\tau = t_1 - t_o$. This step requires only classical communication between neighboring nodes and is traditionally called *particle streaming* in the literature on classical lattice-gas dynamics [14, 15].

The final step, which loops back to the first step of the quantum lattice-gas algorithm, is to reprepare (that is, to “write” once again) the quantum state of the computer according to the prescription (4). Then, we have the updated value of each qubit expressed in terms of the updated values of the occupation probabilities

$$|q'_a(x_l, t_o)\rangle = \sqrt{f'_a(x_{l+e_a}, t_o)}|1\rangle + \sqrt{1 - f'_a(x_{l+e_a}, t_o)}|0\rangle. \quad (10)$$

Setting the updated value of each qubit equal to the value of the qubit at the later time incremented by one unit, $|q(x_l, t_1)\rangle \equiv |q'(x_l, t_o)\rangle$, this final step of the algorithm is equivalently expressed as

$$|q_a(x_l, t_1)\rangle = \sqrt{f_a(x_l, t_1)}|1\rangle + \sqrt{1 - f_a(x_l, t_1)}|0\rangle. \quad (11)$$

As just mentioned, this is identical to the first step of the algorithm given in (4), except that $|q_a\rangle$ is evaluated at the incremented time. In this way, we can continue to iterate forward in time, indefinitely, and make a time-history recording of the occupation probabilities encoded in all the $|q_a\rangle$, which in turn, gives us the temporal evolution of the number density field.

According to the quantum algorithmic four-step procedure, the superposition of states spreads within a lattice cell size $\ell = \|x_l - x_{l+e_a}\|$ entangling only on-site qubits and persists for a duration not greater than update time $\tau = t_1 - t_o$. In practice, in the simplest implementation of the algorithm, this unit of time τ is on the order of the T_1 spin relaxation time of the physical system in questions because this is the time interval needed before state reparation can begin. In the case of the nuclear magnetic resonance type-II quantum computer, T_1 is on the order of 10 seconds. If $T_1 \gg T_2$, this imposes an inefficiency on the type-II quantum computer architecture since much time would be expended waiting for the system to relax back to equilibrium, during which time no useful computation is performed. There are two ways to resolve this inefficiency. First, one can use physical systems where T_1 is greater but on the order of T_2 . Second, if $T_1 \gg T_2$, which is applicable to the NMR case, a “reverse” program could be run to “quickly” force the system to return back to equilibrium. This second solution would only be practical if the original program for the collision operator, the measurement step, and the reverse program, could all be accomplished within a single T_2 time period.

3 Quantum Lattice-Boltzmann Equation

All the algorithmic steps described in the previous section can be encapsulated mathematically in a single finite-difference equation which combines the collision

and streaming operations as well as the measurement process, expressed as a matrix element, as follows

$$f_a(x_{l+e_a}, t_{n+1}) = f_a(x_l, t_n) + \langle \psi(x_l, t_n) | \hat{U}^\dagger \hat{n}_a \hat{U} - \hat{n}_a | \psi(x_l, t_n) \rangle, \quad (12)$$

for $l = 1, 2, \dots, L$, for $n = 0, 1, 2, \dots$, and for $a = 1, 2$. This finite-difference equation is called the *quantum lattice-Boltzmann equation*. It is an exact representation of the factorized quantum lattice-gas dynamics at the mesoscopic scale. The collision term, the last term on the right hand side of (12), can be simplified and written explicitly in terms of the occupation probabilities f_a . To model the Burgers equation, we choose a collision operator that conserves the total on-site occupancy, also referred to as the *particle number* in the literature on lattice gases. That is, of the four basis states enumerated in (2), the collision operator may entangle the first and second qubits at each site by causing a superposition of the states $|01\rangle$ and $|10\rangle$. Therefore, a general representation of the collision operator is a block diagonal matrix, a single U(2) quantum gate

$$\hat{U} = \begin{pmatrix} 1 & 0 & 0 & 0 \\ 0 & e^{i\phi} e^{i\xi} \cos \theta & e^{i\phi} e^{i\xi} \sin \theta & 0 \\ 0 & -e^{i\phi} e^{-i\xi} \sin \theta & e^{i\phi} e^{-i\xi} \cos \theta & 0 \\ 0 & 0 & 0 & \pm 1 \end{pmatrix}. \quad (13)$$

Note that the plus or minus sign of the last component of unitary collision matrix accounts for whether or not the on-site qubits are bosonic (+1) or fermionic (-1) in character [13], but otherwise has no bearing on the resulting kinetic transport equations. Substituting (3) and (13) into (12) gives us explicit update rules for the probability occupancies

$$f'_1 = f_1 f_2 + \left\| e^{i\xi} \cos \theta \sqrt{f_1(1-f_2)} + e^{i\xi} \sin \theta \sqrt{(1-f_1)f_2} \right\|^2 \quad (14)$$

$$f'_2 = f_1 f_2 + \left\| -e^{-i\xi} \sin \theta \sqrt{f_1(1-f_2)} + e^{-i\xi} \cos \theta \sqrt{(1-f_1)f_2} \right\|^2, \quad (15)$$

where the double vertical bars denote the norm or absolute value of the enclosed quantity. After some algebraic manipulation, this pair of equations can be reduced to the standard form

$$f'_a = f_a + \Omega_a, \quad (16)$$

where the collision term, Ω_a , is

$$\Omega_a = -\sin^2 \theta [f_a(1-f_{a+1}) - (1-f_a)f_{a+1}] + \sin 2\theta \cos(\zeta - \xi) \sqrt{f_a(1-f_a)f_{a+1}(1-f_{a+1})}, \quad (17)$$

for $a = 1, 2$. Note that in (17) we use the convention that the subscript of the occupation probability is taken modulo 2; that is, $f_a = f_{\text{mod}_2(a)}$. The quantum lattice-Boltzmann equation expressed in (16) has the traditional form of a kinetic lattice-Boltzmann equation often used in the literature on the classical lattice gases. However, as seen in (17), other than the dependence of the

Euler angles, there appears an unusual dependence on the square root of the occupation probabilities. This type of additional term is a consequence of the microscopic scale quantum nature of the model that remains clearly evident at the mesoscopic scale where (17) is well-defined, even though our quantum algorithm requires periodic and homogenous measurement of all qubits in the computer. In fact, it is just this term that will give rise to non-linearity in the macroscopic equation of motion and that will allow us to model the Burgers equation as we shall demonstrate in §5.

4 Local Equilibrium

Before we derive an effective field theory for the macroscopic scale behavior of our factorized quantum lattice-gas system, it is first necessary to establish the form of the local equilibrium occupancy probabilities, f_a^{eq} . By definition, we know that the collision term (17) must vanish at local equilibrium. For convenience, let us denote the equilibrium occupancy probabilities by $d_1 \equiv f_1^{\text{eq}}$ and $d_2 \equiv f_2^{\text{eq}}$. Then the equilibrium condition $\Omega_a = 0$ is equivalent to

$$\sin^2 \theta [d_1(1 - d_2) - (1 - d_1)d_2] = \sin 2\theta \cos(\zeta - \xi) \sqrt{d_1(1 - d_1)d_2(1 - d_2)}. \quad (18)$$

This may be rewritten in what may be called *detailed-balance form* by dividing the left and right hand sides of the above equation by $d_1(1 - d_1)d_2(1 - d_2)$ giving

$$\frac{d_1}{1 - d_1} - \frac{d_2}{1 - d_2} = 2 \cot \theta \cos(\zeta - \xi) \sqrt{\frac{d_1}{1 - d_1} \frac{d_2}{1 - d_2}}. \quad (19)$$

Our basic approach is that the equilibrium occupancy probabilities can be parameterized in the following way

$$d_1 = \frac{1}{e^{\beta E_1} + 1} \quad \text{and} \quad d_2 = \frac{1}{e^{\beta E_2} + 1}. \quad (20)$$

Letting $\beta E + \ln \gamma \equiv \beta E_1$ and $E - \ln \gamma \equiv \beta E_2$, we can write

$$d_1 = \frac{1}{\gamma e^{\beta E} + 1} \quad \text{and} \quad d_2 = \frac{1}{\frac{1}{\gamma} e^{\beta E} + 1}. \quad (21)$$

Expressed in terms of E and γ , the equilibrium condition (19) then becomes

$$\frac{1}{\gamma} e^{-\beta E} - \gamma e^{-\beta E} = 2 \cot \theta \cos(\zeta - \xi) e^{-\beta E}, \quad (22)$$

which simplifies to the following quadratic equation

$$\gamma^2 + 2 \cot \theta \cos(\zeta - \xi) \gamma - 1 = 0. \quad (23)$$

We take the positive root for our solution so that d_1 and d_2 in turn are positive

$$\gamma = \sqrt{\cot^2 \theta \cos^2(\zeta - \xi) + 1} - \cot \theta \cos(\zeta - \xi). \quad (24)$$

For convenience, let us label the trigonometric factor $\alpha \equiv \cot \theta \cos(\zeta - \xi)$. Then we have

$$\gamma = \sqrt{\alpha^2 + 1} + \alpha \quad \text{and} \quad \frac{1}{\gamma} = \sqrt{\alpha^2 + 1} - \alpha. \quad (25)$$

Now the equilibrium number density $\rho = d_1 + d_2$ gives us the following relation between ρ , γ , and the fugacity $e^{\beta E}$

$$\rho = \frac{1}{\gamma e^{\beta E} + 1} + \frac{1}{\frac{1}{\gamma} e^{\beta E} + 1}. \quad (26)$$

After some algebraic manipulation, this can be rewritten as a quadratic equation in the fugacity

$$\rho e^{2\beta E} + \left(\gamma + \frac{1}{\gamma} \right) (\rho - 1) e^{\beta E} + \rho - 2 = 0. \quad (27)$$

The solutions are

$$e^{\beta E} = \frac{1}{2} \left(\gamma + \frac{1}{\gamma} \right) \frac{1 - \rho}{\rho} \pm \frac{1}{\rho} \sqrt{\frac{1}{4} \left(\gamma + \frac{1}{\gamma} \right)^2 (1 - 2\rho + \rho^2) - \rho^2 + 2\rho}. \quad (28)$$

Now from (25) we see that $\left(\gamma + \frac{1}{\gamma} \right) = 2\sqrt{\alpha^2 + 1}$. Taking the positive root of (28), we then have

$$e^{\beta E} = \frac{1 - \rho}{\rho} \sqrt{\alpha^2 + 1} + \frac{1}{\rho} \sqrt{(\alpha^2 + 1)(1 - 2\rho + \rho^2) - \rho^2 + 2\rho}. \quad (29)$$

We had to take the positive root to be consistent with the classical case where the only possible collision term is $\Omega_a = -f_a(1 - f_{a+1}) + (1 - f_a)f_{a+1}$, which is deterministic. The classical collision term corresponds to the case in the quantum lattice-gas model (17) where $\alpha = 0$. In the classical case, the occupation probabilities must be equal, so $\rho = 2d = \frac{2}{e^{\beta E} + 1}$, which in turn means that $e^{\beta E} = \frac{1 - \rho}{\rho} + \frac{1}{\rho}$. This is consistent with expression (29).

Given the solution (29), we in turn may express the equilibrium probability of occupancies in terms of the number density. That is, substituting (29) into (21), and after performing some algebraic reduction, we have

$$\begin{aligned} d_1 &= \frac{\rho}{2} + \frac{1}{2\alpha} \sqrt{\alpha^2 + 1} - \frac{1}{2\alpha} \sqrt{(\alpha^2 + 1) - 2\alpha^2\rho + \alpha^2\rho^2} \\ d_2 &= \frac{\rho}{2} - \frac{1}{2\alpha} \sqrt{\alpha^2 + 1} + \frac{1}{2\alpha} \sqrt{(\alpha^2 + 1) - 2\alpha^2\rho + \alpha^2\rho^2}. \end{aligned} \quad (30)$$

Therefore, in the quantum lattice-gas model, the equilibrium occupancy probabilities are not equal, except for the two trivial cases where the number density is either completely empty $\rho = 0$ or completely full $\rho = 2$. This characteristic of non-equal occupations, while satisfying a detail-balance condition (19), is a characteristic unique to quantum lattice-gas models. This is not possible with any kind of classical lattice-gas model with strictly local interactions.

5 The Burgers Equation

We can explicitly rewrite the mesoscopic transport equation (16) as

$$\begin{aligned} f'_1 &= f_1 \cos^2 \theta + f_2 \sin^2 \theta + \sin 2\theta \cos(\zeta - \xi) \sqrt{f_1(1-f_1)f_2(1-f_2)} \\ f'_2 &= f_1 \sin^2 \theta + f_2 \cos^2 \theta - \sin 2\theta \cos(\zeta - \xi) \sqrt{f_1(1-f_1)f_2(1-f_2)}, \end{aligned} \quad (31)$$

where for brevity the dependence on x_l and t_n of each occupancy probability is omitted. Using these strictly local transport equations, we can derive an effective field theory that accurately and precisely describes the dynamical behavior of our quantum lattice-gas model at the macroscopic scale.

We begin our derivation with the simplest case where deviation of the quantum occupancy probabilities are close to the classical value $f_a^{\text{eq}} \simeq \frac{\rho}{2}$, for $a = 1, 2$. From the equilibrium solutions (30), we see that the system approaches the classical regime when the trigonometric factor α is small. To calculate a finite-difference expression for the number density, we must express the number density field at the new incremented time t_{n+1}

$$\rho(x_l, t_{n+1}) = f_1(x_l, t_{n+1})|_{f_1 \simeq \frac{\rho}{2}} + f_2(x_l, t_{n+1})|_{f_2 \simeq \frac{\rho}{2}}, \quad (32)$$

in terms of the number density field evaluated at the previous time t_n . This can be accomplished by substituting the equilibrium values into (31) to give us

$$\begin{aligned} f'_1(x_l, t_n) &= \frac{\rho(x_l, t_n)}{2} + \sin 2\theta \cos(\zeta - \xi) \frac{\rho(x_l, t_n)}{2} \left(1 - \frac{\rho(x_l, t_n)}{2}\right) \\ f'_2(x_l, t_n) &= \frac{\rho(x_l, t_n)}{2} - \sin 2\theta \cos(\zeta - \xi) \frac{\rho(x_l, t_n)}{2} \left(1 - \frac{\rho(x_l, t_n)}{2}\right). \end{aligned} \quad (33)$$

Using the streaming rule (9), we can rewrite these two update equation as

$$\begin{aligned} f_1(x_l, t_{n+1}) &= \frac{\rho(x_{l+1}, t_n)}{2} + \sin 2\theta \cos(\zeta - \xi) \frac{\rho(x_{l+1}, t_n)}{2} \left(1 - \frac{\rho(x_{l+1}, t_n)}{2}\right) \\ f_2(x_l, t_{n+1}) &= \frac{\rho(x_{l-1}, t_n)}{2} - \sin 2\theta \cos(\zeta - \xi) \frac{\rho(x_{l-1}, t_n)}{2} \left(1 - \frac{\rho(x_{l-1}, t_n)}{2}\right). \end{aligned} \quad (34)$$

Now substituting these expressions into (32), after some algebraic simplifications we have the following governing nonlinear finite-difference equation

$$\begin{aligned} \rho(x_l, t_{n+1}) - \rho(x_l, t_n) &= \frac{1}{2} [\rho(x_{l+1}, t_n) - 2\rho(x_l, t_n) + \rho(x_{l-1}, t_n)] \\ &\quad + \frac{1}{2} \sin 2\theta \cos(\zeta - \xi) [\rho(x_{l+1}, t_n) - \rho(x_{l-1}, t_n)] \\ &\quad - \frac{1}{4} \sin 2\theta \cos(\zeta - \xi) [\rho(x_{l+1}, t_n)^2 - \rho(x_{l-1}, t_n)^2], \end{aligned} \quad (35)$$

where $\rho(x_l, t_n)$ has been subtracted from both the left and right hand sides. Note that (35) embodies an explicit numerical scheme because all the terms on the R.H.S. depend only on t_n .

In the continuum limit where the lattice spacing and the update time both approach zero, the number density field becomes continuous and differentiable. Then the L.H.S. of the governing difference equation becomes the first partial derivative with respect to time, the first term on the R.H.S. becomes one-half the second partial derivative of the number density field with respect to space, and the second term on the R.H.S. becomes proportional to the first partial derivative with respect to space. The last term on the R.H.S. is a bit more difficult to interpret by inspection in the continuum limit, but nevertheless is straightforward to evaluate. We use the expansion $\rho(x \pm \delta x) \simeq \rho(x) \pm 2\rho(x) \frac{\partial \rho(x)}{\partial x} \delta x + \left[\frac{\partial \rho(x)}{\partial x} \right]^2 \delta x^2$ to evaluate this last term, and then it follows that the governing difference equation (35) approximates the following nonlinear partial differential equation in the continuum limit

$$\frac{\partial \rho(x, t)}{\partial t} + c \sin 2\theta \cos(\zeta - \xi) [\rho(x, t) - 1] \frac{\partial \rho(x, t)}{\partial x} = \frac{1}{2} \frac{\ell}{\tau} \frac{\partial^2 \rho(x, t)}{\partial x^2}. \quad (36)$$

This is the nonlinear Burgers equation.

6 Numerical Simulation

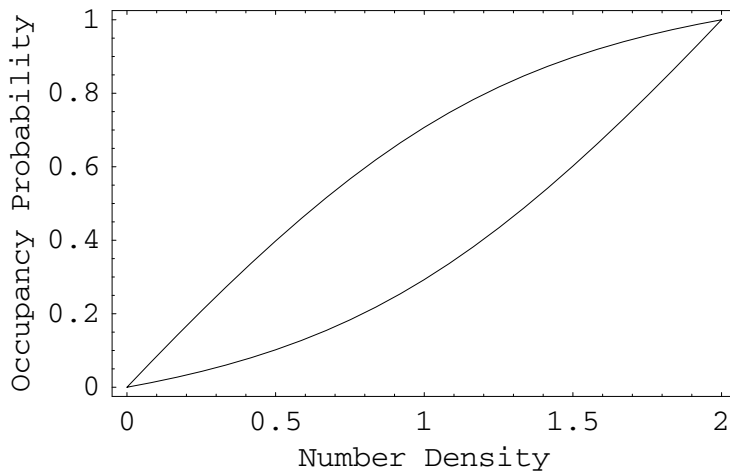


Figure 1: A plot of the occupancy probabilities of the two on-site qubits versus the number density at that site. The upper curve is f_1^{eq} and the lower curve is f_2^{eq} as specified by (38). In a quantum lattice gas, the occupancy probabilities can be different while the system nevertheless obeys a detailed-balance condition. The abscissa and ordinate are both non-dimensional probability values.

If we choose the ‘‘Euler’’ angles in (13) to be $\phi = 0$, $\theta = \frac{\pi}{4}$, $\xi = \zeta$, then the general collision operator reduces the quantum gate

$$\hat{U} = \begin{pmatrix} 1 & 0 & 0 & 0 \\ 0 & \frac{1}{\sqrt{2}} & \frac{1}{\sqrt{2}} & 0 \\ 0 & -\frac{1}{\sqrt{2}} & \frac{1}{\sqrt{2}} & 0 \\ 0 & 0 & 0 & \pm 1 \end{pmatrix}. \quad (37)$$

In this particular case, the equilibrium occupations are

$$f_a^{\text{eq}} = \frac{\rho}{2} + \frac{e_a}{\sqrt{2}} \left[1 - \sqrt{1 - \left(\frac{\rho}{2}\right) \left(1 - \frac{\rho}{2}\right)} \right], \quad (38)$$

and are plotted in Figure 1. The mesoscopic transport equation (16) reduces to the simpler form

$$\begin{aligned} f_1' &= f_1 - \frac{1}{2}[f_1(1-f_2) - (1-f_1)f_2] + \sqrt{f_1(1-f_1)f_2(1-f_2)} \\ f_2' &= f_2 + \frac{1}{2}[f_1(1-f_2) - (1-f_1)f_2] - \sqrt{f_1(1-f_1)f_2(1-f_2)}, \end{aligned} \quad (39)$$

and macroscopic equation of motion (36) reduces to the following parabolic partial differential equation

$$\frac{\partial \rho}{\partial t} + c \frac{\partial}{\partial x} \left(\rho - \frac{\rho^2}{2} \right) = \frac{\ell^2}{2\tau} \frac{\partial^2 \rho}{\partial x^2}. \quad (40)$$

Setting $u \equiv c(\rho - 1)$, we then have the Burgers equation in standard form

$$\frac{\partial u}{\partial t} - u \frac{\partial u}{\partial x} = \nu \frac{\partial^2 u}{\partial x^2}, \quad (41)$$

where $\nu = \frac{\ell^2}{2\tau}$ is the transport coefficient.⁶

To test the prediction that the macroscopic scale behavior of the quantum lattice-gas model is governed by the Burgers equation (41), one may compare the results of the numerical simulation to an exact solution obtained by analytical means. In a different context, this type of comparison was done by Boghosian and Levermore in 1987 when they tested the accuracy and efficiency of their classical lattice-gas model of the Burgers equation [31]. The presentation in this section follows their numerical test procedure. For the purposes of the numerical test, the system is simulated directly at the mesoscopic scale using (39), and initialized with a sinusoidal profile in the number density field

$$\rho(x_l, 0) = \rho_a \cos\left(\frac{2\pi l}{L}\right) + \rho_b, \quad (42)$$

⁶ It is possible to add an external noise term into the right-hand side of the Burgers equation (41) of the form $\frac{\partial \eta(x,t)}{\partial x}$. We define the potential field $h(x,t)$ as follows: $\frac{\partial h(x,t)}{\partial x} \equiv u(x,t)$. Then $h(x,t)$ satisfies the Kardar-Parisi-Zhang equation [30].

where $\rho_a = 0.4$ and $\rho_b = 1$, and $L = 256$. A time history of the dynamical evolution of the the number density field is plotted in blue in Figure 2.

An analytical solution of the Burgers equation can be obtained by application of the Cole-Hopf transformation

$$\rho = \rho_a + \frac{2\nu}{c\psi} \frac{\partial\psi}{\partial x}, \quad (43)$$

where

$$\psi \equiv I_0(z) + 2 \sum_{\ell=1}^{\infty} (-1)^{\text{Floor}[\ell/2]} I_{\ell}(z) f_{\ell}(2\pi\ell x + \nu_{\ell}t) e^{-\mu_{\ell}t}, \quad (44)$$

and where $z \equiv \frac{c\rho_b}{4\pi\nu}$, $\mu_{\ell} \equiv \nu(2\pi\ell)^2$, $\nu_{\ell} \equiv c(\rho_a - 1)(2\pi\ell)$, the I_{ℓ} 's are modified Bessel functions, and the function f_{ℓ} denotes the sine or cosine function when ℓ is odd or even, respectively,

$$f_{\ell}(x) \equiv \frac{(-1)^{\ell} + 1}{2} \cos(x) - \frac{(-1)^{\ell} - 1}{2} \sin(x). \quad (45)$$

To match the numerical simulation, the parameters in the analytical solution (44) were set to $c = L = 256$ and $\nu = \frac{1}{2}$. The agreement between the numerical prediction and the analytical solution is excellent, as shown in Figure 2. There is a slight discrepancy between the two results after the shock front has fully developed in the number density field. The discrepancy occurs at the corners or edges of the shock. The analytical solution appears to be smoother across the shock front than the numerical solution. To plot the analytical solution, it was not possible to include all terms in the series expansion (44) from $\ell = 1$ up to $\ell = \infty$. Instead, an accurate approximation was made where the first 80 terms in the expansion (44) were used. The numerical error incurred by truncating the expansion in this way is less than the round-off error of the least significant bit of a double-precision floating-point representation, and therefore does not account for the observed discrepancy at the edges of the shock front.

7 Conclusion

This paper presented a factorized quantum lattice-gas algorithm for modeling the nonlinear Burgers equation. The quantum algorithm was developed for direct implementation on a type-II quantum computer and is primarily intended for that purpose. All algorithmic steps were enumerated. A derivation of the mesoscopic scale transport equation, a quantum lattice-Boltzmann equation, was presented, as was a derivation of the macroscopic scale effective field theory governing the number density field. A general parabolic and nonlinear partial differential equation, in the form of the Burgers equation, was the predicted governing equation of motion. The results of a numerical simulation of the model were then presented along with a comparison to the exact analytical solutions for the problem of shock formation given an initial sinusoid profile in the number density field. The agreement of the analytical predictions to the

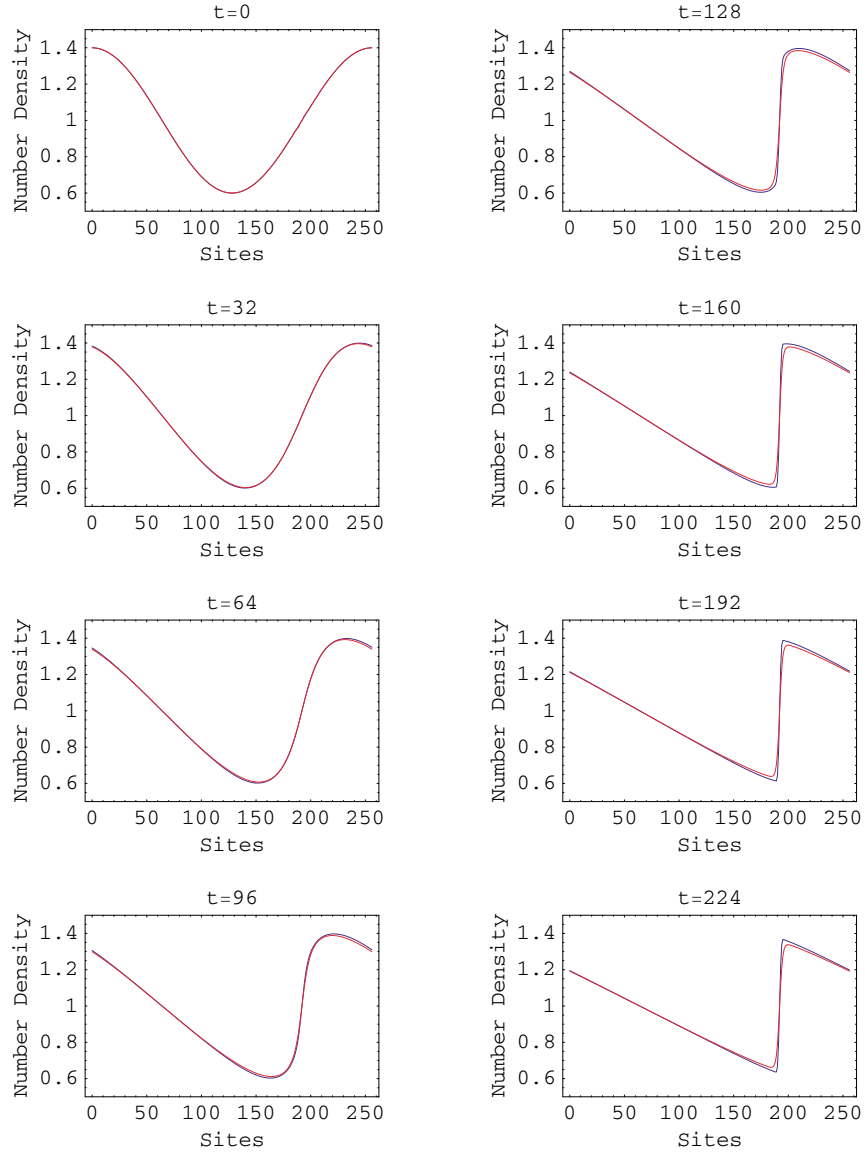


Figure 2: Development of a shock front in the number density field after the system was initialized with a sinusoidal profile on a $L = 256$ site lattice. Agreement between the numerical data (blue curve) and the analytical solution (red) curve is apparent. However, the analytical solution appears to depart from the numerical solution at later times when a steep shock front is fully formed. The edges of the analytical solution are smooth compared to the sharp edges of the numerical simulation.

numerically predicted solutions was excellent confirming the analytically derived effective theory is indeed the correct one.

The efficiency of the factorized quantum lattice-gas algorithm is significantly better than its classical lattice-gas algorithm counterpart when judged strictly on classical numerical modeling grounds and when both algorithms are implemented on the same general purpose computer (such as a desktop personal computer).⁷ The classical lattice-gas algorithm for the Burgers equation was one of the first classical lattice-gas algorithms ever presented [31] that was carefully tested against an exact analytical solution to the partial differential equation the lattice-gas system was supposed to model. In the case of the classical lattice-gas model, significant computational resources were expended to observe shock formation. That is, to obtain reasonably accurate mesoscopic data in the classical lattice-gas model, course-grain averaging over blocks of size 512 lattice sites was required. The entire lattice size for the classical lattice-gas model required a rather large simulation space of 65536 sites, and the characteristic time for shock formation was on the order of $2^{18} = 262144$ time steps. In contrast, the quantum lattice-gas model reproduced a cleaner approximation of the dynamical formation of the shock using a small lattice of only 256 sites in less than 256 time steps. This substantial reduction in required computational resources was possible because the mesoscopic transport equations could be accurately modeled directly on a classical computer in a numerically unconditionally stable fashion that obeyed the principle of detailed-balance.

It is possible to apply the quantum lattice-gas algorithmic method to multi-dimensional situations. In two and three dimensions, it is possible to recover the nonlinear convective term associated with the Burgers equation. However, in this situation, there also appears a pressure term, so the resulting macroscopic partial differential equation is the Navier-Stokes equations. If an inter-particle potential is applied (by using non-local collisions), in principle it would be possible to cancel the gradient pressure term and therefore recover the Burgers equation in two or three dimensions. It is presently an open question as to whether or not it is possible to recover the Burgers equation in two or three dimensions by using only local particle collisions.

⁷ The finite-difference lattice-Boltzmann equation (39) is suited to standard general purpose computers with floating-point arithmetic processors, a computational resource not needed by the classical lattice-gas algorithm, so the claim for improved computational efficiency of the lattice-Boltzmann method over the classical lattice-gas method could be made stronger. Using special-purpose hardware such as the CAM-8 machine [32], with a total cost of all its simple components no more costly than the components in a conventional personal computer, it is possible to speed up the execution of classical lattice-gas models by several orders of magnitude. Yet even this degree of speedup does not give a competitive advantage to hydrodynamic classical lattice-gas algorithms (of which the Burgers equation is a special case) running on special purpose hardware [33]. However, it has been demonstrated that the lattice-Boltzmann method is a competitive computational fluid dynamics solver, for example, when compared with the spectral method [34].

A Scaling Estimate for the Minimum Ensemble Size

We can estimate the minimum number of repeated measurements that are required to evaluate the occupancy probabilities to a sufficient precision for the quantum lattice-gas to accurately model turbulent hydrodynamic flow. The argument begins with the following principle: there is equivalence between ensemble averaging over independent replicas and coarse-grain block averaging over space. In an NMR quantum computer implementation of a type-II quantum computer, one would use ensemble averaging to evaluate the occupation probabilities and not coarse-grain averaging. However, we know that the total number of nodes, n , needed in a single coarse-grain block scales as $n \sim \frac{\text{Re}^{\frac{1}{2}}}{M^2}$, where Re is the Reynolds number and M is the Mach number [33]. By the equivalence principle, we will therefore require n replicas to comprise our ensemble. The total number of cells, L^3 , needed to resolve a three-dimensional turbulent eddy down to the dissipation scale goes as $L^3 \sim \text{Re}^{\frac{9}{4}}$ [33]. Therefore, the minimum size of the ensemble can be expressed as $n \sim \frac{L^{\frac{2}{3}}}{M^2}$. For a turbulent simulation with a Reynolds number of a million, then the ensemble size should be much greater than about 10^5 , given a small Mach number of about one tenth. This is not too large of an ensemble size to make the type-II quantum computation impractical. Furthermore, simulating the Navier-Stokes equation in its turbulence regime is more difficult than simulating shock formation governed by the Burgers equation.

References

- [1] S.F. Shandarin and Ya. B. Zeldovich. The large-scale structure of the universe: Turbulence, intermittency, structures in a self-gravitating medium. *Reviews of Modern Physics*, 61(2):185–220, 1989.
- [2] E. Ben-Naim, S.Y. Chen, G.D. Doolen, and S. Redner. Shocklike dynamics of inelastic gases. *Physical Review Letters*, 83(20):4069–4072, 1999.
- [3] Jeffrey Yepez. Type-ii quantum computers. *International Journal of Modern Physics C*, 12(9):1–12, 2001. Presented at the Quantum Computing Colloquium, MIT Nuclear Engineering Department, September 27, 1999 and at the Air Force Office of Scientific Research Computational and Applied Mathematics Meeting 2000, Stanford University, June 28, 2000.
- [4] Jeffrey Yepez. Lattice-gas quantum computation. *International Journal of Modern Physics C*, 9(8):1587–1596, 1998. Proceeding of the 7th International Conference on the Discrete Simulation of Fluids, University of Oxford.
- [5] Jeffrey Yepez. Quantum computation of fluid dynamics. In Collin P. Williams, editor, *Quantum Computing and Quantum Communications*,

page 480pp. Lecture Notes in Computer Science, Springer-Verlag, 1999. First NASA International Conference, QCQC'98, Palm Springs, California, USA, February 17-20, 1998, Selected Papers.

- [6] Jeffrey Yepez. Quantum lattice-gas model for the diffusion equation. *International Journal of Modern Physics C*, 12(9):1–19, 2001. Presented at the 9th International Conference on Discrete Simulation of Fluid Dynamics, Santa Fe, NM, August 22, 2000.
- [7] Sauro Succi and R. Benzi. Lattice boltzmann equation for quantum mechanics. *Physica D*, 69:327–332, 1993.
- [8] Sauro Succi. Numerical solution of the schrodinger equation using discrete kinetic theory. *Physical Review E*, 53(2):1969–1975, 1996.
- [9] Iwo Bialynicki-Birula. Weyl, dirac, and maxwell equations on a lattice as unitary cellular automata. *Physical Review D*, 49(12):6920–6927, 1994.
- [10] David A. Meyer. From quantum cellular automata to quantum lattice gas. *Journal of Statistical Physics*, 85(5,6):551–574, 1996.
- [11] David A. Meyer. Quantum mechanics of lattice gas automata: One-particle plane waves and potentials. *Physical Review E*, 55(5):5261–5269, 1997.
- [12] Bruce M. Boghosian and Washington Taylor IV. Quantum lattice gas models for the many-body schrodinger equation. *International Journal of Modern Physics C*, 8:705–716, 1997.
- [13] Jeffrey Yepez. A quantum lattice-gas model for computational fluid dynamics. *Physical Review E*, (046702):046702–1 to 046702–18, 2001. APS E-Print: aps1999Oct22_002.
- [14] Uriel Frisch, Brosl Hasslacher, and Yves Pomeau. Lattice-gas automata for the navier-stokes equation. *Physical Review Letters*, 56(14):1505–1508, 1986.
- [15] Uriel Frisch, Dominique d’Humières, Brosl Hasslacher, Pierre Lallemand, Yves Pomeau, and Jean-Pierre Rivet. Lattice gas hydrodynamics in two and three dimensions. *Complex Systems*, 1:649–707, 1987.
- [16] Bruce M. Boghosian, Jeffrey Yepez, Francis J. Alexander, and Norman H. Margolus. Integer lattice gas. *Physical Review E*, 55(4):4137–4147, 1997. comp-gas/9602001.
- [17] M.H. Ernst and Shankar P. Das. Thermal cellular automata fluids. *Journal of Statistical Physics*, 66(1/2):465–483, 1992.
- [18] Chenghai Sun. Lattice-boltzmann models for high speed flows. *Physical Review E*, 58(6):7283–7287, 1998.

- [19] Cécile Appert and Stéphane Zaleski. Lattice gas with a liquid-gas transition. *Physical Review Letters*, 64:1–4, 1990.
- [20] Jeffrey Yepez. Lattice-gas crystallization. *Journal of Statistical Physics*, 81(1/2):255–294, 1994.
- [21] Andrew N. Emerton, Peter V. Coveney, and Bruce M. Boghosian. Lattice-gas simulations of domain growth, saturation, and self-assembly in immiscible fluids and microemulsions. *Physical Review E*, 56(1):1286, 1997.
- [22] Ray Kapral, Anna Lawniczak, and P. Masiar. Oscillations and waves in a reactive lattice-gas automaton. *Physical Review Letters*, 66:2539–2542, 1991.
- [23] J.A. Jones and E. Knill. Efficient refocusing of one-spin and two-spin interactions for nmr quantum computation. *Journal of Magnetic Resonance*, 141(2):322–5, 1999.
- [24] David G. Cory, Amr F. Fahmy, and Timothy F. Havel. Ensemble quantum computing by nuclear magnetic resonance spectroscopy. In Tommaso Toffoli, Michael Biafore, and J. Le ao, editors, *PhysComp 96*, pages 87–91. Proceedings on the Fourth Workshop on Physics and Computation, New England Complex Systems Institute, 1996.
- [25] David G. Cory, Mark D. Price, and Timothy F. Havel. Nuclear magnetic resonance spectroscopy: An experimentally accessible paradigm for quantum computing. *Physica*, D(120):82–101, 1998.
- [26] J.E. Mooij, Terry P. Orlando, L. Levitov, Lin Tian, Casper H. van der Wal, and Seth Lloyd. Josephson persistent-current qubit. *Science*, 285:1036–1039, 1999.
- [27] T.P. Orlando, J.E. Mooij, Lin Tian, Caspar H. van der Wal, L.S. Levitov, Seth Lloyd, and J.J. Mazo. Superconducting persistent-current qubit. *Physical Review B*, 60(22):15398–15413, 1999.
- [28] Jeffrey Yepez and Bruce Boghosian. An efficient and accurate quantum lattice-gas model for the many-body schrodinger wave equation. *Computer Physics Communications*, To Appear 2002.
- [29] David P. DeVincenzo. Two-bit gates are universal for quantum computation. *Physical Review A*, 51:1015–1022, 1995.
- [30] Mehran Kardar, Giorgio Parisi, and Yi-Cheng Zhang. Dynamic scaling of growing interfaces. *Physical Review Letters*, 56(9):889–892, 1986.
- [31] Bruce M. Boghosian and C. David Levermore. A cellular automaton for burger’s equation. *Complex Systems*, 1:17–29, 1987.

- [32] Norman Margolus. Cam-8: a computer architecture based on cellular automata. *American Mathematical Society*, 6, 1996. Fields Institute Communications.
- [33] Steven A. Orszag and Victor Yakhot. Reynolds number scaling of cellular-automaton hydrodynamics. *Physical Review Letters*, 56(16):1691–1693, 1986.
- [34] Danial O. Martinez, William H. Matthaeus, Shiyi Chen, and Dave Montgomery. Comparison of spectral method and lattice bolzmann simulations of two-dimensional hydrodynamics. *Physics of Fluids*, 6(3):1285–1298, 1994.